Corrosion Science 52 (2010) 2905–2916

Contents lists available at ScienceDirect

Corrosion Science

journal homepage: www.elsevier.com/locate/corsci

Electrochemical investigation and modeling of corrosion inhibition of aluminum in molar nitric acid using some sulphur-containing amines

K.F. Khaled *

Electrochemistry Research Laboratory, Ain Shams University, Faculty of Education, Chemistry Department, Roxy, Cairo, Egypt
Materials and Corrosion Laboratory, Taif University, Faculty of Science, Chemistry Department, Taif, Hawiya 888, Saudi Arabia

ARTICLE INFO

Article history:
Received 15 March 2010
Accepted 5 May 2010
Available online 8 May 2010

Keywords:
A. Aluminum
B. EIS
B. Polarization
B. Modeling studies
C. Acid corrosion

ABSTRACT

Chemical and electrochemical measurements incorporated with quantum chemical calculations and molecular dynamics simulations were used to study the corrosion inhibition characteristics of some thiosemicarbazone derivatives on the inhibition of aluminum corrosion in 1.0 M HNO_3. Polarization curves demonstrated that the thiosemicarbazone derivatives were of mixed-type inhibitors. EIS plots indicated that the addition of thiosemicarbazone derivatives increases the charge-transfer resistance of the corrosion process, and hence the inhibition performance. The molecular dynamics simulation results show that the three thiosemicarbazone derivatives can adsorb on the A_2O_3 (1 1 1) surface through the sulphur and nitrogen atoms as well as π-electrons in the pyridyl structure.

1. Introduction

Aluminum is a metal with a high electronegative potential ($-1.67\ V_{SHE}$); in spite of this, it is highly resistant to most acidic and neutral solutions due to the formation of a protective oxide film on its surface. In oxidizing environments the film formation is very rapid and attack on the metal is negligible. This is the reason why very little attention has been paid to the corrosion of aluminum in nitric acid. In a number of industrial processes, such as manufacturing of nitric acid-based explosive, catalytic decomposition of ammonia, and processing of ammonium nitrate, aluminum frequently comes into the contact with nitric acid. Nitric acid of very low and very high concentrations has very little effect on the corrosion of aluminum, but in a concentration range 20–40%, the rate of corrosion is of the order of 4.0 mm y^{-1} even at room temperature, and an increase in the temperature causes severe corrosion of the metal [1]. Therefore, it was considered necessary to seek inhibitors for corrosion of aluminum in nitric acid. Mears and Eldredge [2] have proposed that organic substances could not be used as corrosion inhibitors in nitric acid because the compounds might be decomposed if added to this acid, due to its strong oxidizing nature. Inorganic inhibitors as chromates are effective corrosion inhibitors for aluminum in nitric acid, but they are effective only at very high concentrations and may cause localized attack if used in insufficient amount. Besides these chromates are toxic and also cause pollution. Singh et al. [3–6], investigated some organic compounds as corrosion inhibitors for aluminum in nitric acid and they found that sulphur-containing compounds like thiourea are more effective corrosion inhibitors than nitrogen-containing compounds.

Although, in recent years, some new techniques have been applied to the experimental studies of corrosion inhibitors [7,8], the theoretical approach to this problem is still mostly traditional and confined to quantum chemical calculations involving isolated inhibitor molecules [9–11] and to some extent to the interaction of inhibitor molecules with surface atoms through semi-empirical and ab initio methods [12–15]. Thus in the field of theoretical investigation of corrosion inhibitors, development of more realistic models based on inhibitor located in electrical double layer at metal/solution interface, seems to be in demand. The models applied here take into account substrate, solvent and electric field, are treated quantum chemically by suitable ab initio method at density functional theory (DFT) level.

The aim of this study is to investigate the inhibitive properties of three selected thiosemicarbazone derivatives, namely 3-pyridinecarboxaldehyde thiosemicarbazone (META), isonicotinaldehyde thiosemicarbazone (PARA) and 2-pyridine carboxaldehyde thiosemicarbazone (ORTHO) on the inhibition of aluminum corrosion in 1.0 M HNO_3 solutions using chemical (weight loss) and electrochemical (polarization and impedance) techniques. Also, this study aims to use Metropolis Monte Carlo simulation method to search for adsorption configurations of the studied compounds

* Permanent address: Electrochemistry Research Laboratory, Ain Shams University, Faculty of Education, Chemistry Department, Roxy, Cairo, Egypt.
E-mail address: khaledrice2003@yahoo.com

0010-938X/$ - see front matter © 2010 Elsevier Ltd. All rights reserved.
doi:10.1016/j.corsci.2010.05.001

on Al_2O_3 (1 1 1) surface to find the low energy adsorption sites on the aluminum surface and to investigate the preferential adsorption of the studied thiosemicarbazone derivatives.

2. Experimental

The thiosemicarbazone derivatives used in this study are as follow:

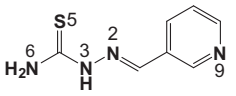

3-Pyridinecarboxaldehyde thiosemicarbazone (META)

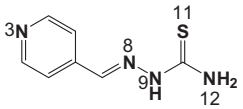

Isonicotinaldehyde thiosemicarbazone (PARA)

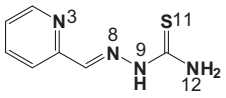

2-Pyridinecarboxaldehyde thiosemicarbazone (ORTHO)

All of these compounds were obtained from Aldrich chemical co. They were added to the 1.0 M HNO_3 (Fisher Scientific) without pre-treatment at concentrations of 10^{-4}, 10^{-3}, 5×10^{-3} and 10^{-2} M.

Cylindrical rods of aluminum specimens obtained from Johnson Mattey (Puratronic, 99.999%) were mounted in Teflon. An epoxy resin was used to fill the space between Teflon and aluminum electrode. The circular cross sectional area of the aluminum rod exposed to the corrosive medium, used in electrochemical measurements, was (0.28 cm^2). Weight loss measurements were carried out using the same aluminum rods, each of 2.50 cm length and 0.5 cm diameter (surface area = 3.925 cm^2). The weight loss experiments were carried out in 500 ml Corning glass beakers (without lid) containing 250 ml of the electrolyte (1.0 M HNO_3). The inhibitor efficiencies were evaluated after a period of 48 h using 10^{-4}, 10^{-3}, 5×10^{-3} and 10^{-2} M of thiosemicarbazone derivatives. After removing the specimens from the electrolyte, they were kept for 3–4 min. in 70% nitric acid, washed thoroughly with distilled water and then dried and weighed. The electrochemical measurements were performed in a typical three-compartment glass cell consisted of the aluminum specimen as working electrode (WE), platinum counter electrode (CE) and a saturated calomel electrode (SCE) as the reference electrode. The counter electrode was separated from the working electrode compartment by fritted glass. The reference electrode was connected to a Luggin capillary to minimize IR drop. Solutions were prepared from bidistilled water of resistivity 13 M Ω cm. The exposed area of the aluminum electrode was mechanically abraded with 800, 1200, 1500 and 2000 grades of emery papers, degreased with acetone and rinsed by distilled water and finally dried before each experiment.

The electrode potential was allowed to stabilize 60 min before starting the measurements. All experiments were conducted at 25 ± 1 °C. The electrolyte solution was made from HNO_3 (Fisher Scientific) and bidistilled water. The inhibitors (Aldrich chemical co.) used without any pre-treatments. Measurements were performed using Gamry Instrument Potentiostat/Galvanostat/ZRA. This includes a Gamry Framework system based on the ESA400, Gamry applications that include dc105 for dc corrosion measurements, EIS300 for electrochemical impedance spectroscopy measurements along with a computer for collecting data. Echem Analyst 5.58 software was used for plotting, graphing and fitting data.

Tafel polarization curves were obtained by changing the electrode potential automatically from (−900 to −400 mV_{SCE}) at open circuit potential with scan rate of 1.0 mV s^{-1}. Impedance measurements were carried out in frequency range from 10 kHz to 1.0 mHz with an amplitude of 10 mV peak-to-peak using ac signals at open circuit potential.

3. Computational details

There is increasing number of publications attempting to correlate the structure of corrosion inhibitors. Their state of adsorption at the metal/solution interfaces and inhibition effectiveness are appearing in the literature. The semi-empirical computational methods have been used most successfully in finding correlation between theoretically calculated properties and experimentally determined inhibition efficiency for uniform corrosion [16–26]. The electronic properties of inhibitors, effects of the frontier molecular orbital energies, the differences between lowest unoccupied molecular orbital (LUMO) and highest occupied molecular orbital (HOMO) energies ($E_L - E_H$), electronic charges on the reactive centers, dipole moments and conformation of molecules have been investigated. No application of semi-empirical methods in studying of inhibition of pitting corrosion has been reported yet. In the present study, we are reporting on some attempts to elucidate the inhibition mechanism of thiosemicarbazone derivatives for the corrosion of aluminum in 1.0 M HNO_3 by using semi-empirical methods as well as molecular dynamics simulation techniques. Thiosemicarbazone derivatives have been simulated as adsorbate on Al_2O_3 (1 1 1) substrate to find the low energy adsorption sites on the aluminum surface and to investigate the preferential adsorption of the studied thiosemicarbazone derivatives. The geometry optimization process is carried out for the studied thiosemicarbazone derivatives using an iterative process, in which the atomic coordinates are adjusted until the total energy of a structure is minimized, i.e., it corresponds to a local minimum in the potential energy surface. The forces on the atoms in the thiosemicarbazone derivatives are calculated from the potential energy expression and will, therefore, depend on the force field that is selected.

Interaction between thiosemicarbazone derivatives and Al_2O_3 (1 1 1) surface was carried out in a simulation box (14.27 Å × 14.27 Å × 14.27 Å) with periodic boundary conditions to model a representative part of the interface devoid of any arbitrary boundary effects. The Al_2O_3 (1 1 1) was first built and relaxed by minimizing its energy using molecular mechanics, then the surface area of Al_2O_3 (1 1 1) was increased and its periodicity is changed by constructing a super cell, and then a vacuum slab with 50 Å thicknesses was built on the Al_2O_3 (1 1 1) surface. The number of layers in the structure was chosen so that the depth of the surface is greater than the non-bond cutoff used in calculation. Using six layers of Al_2O_3 atoms gives a sufficient depth that the inhibitor molecules will only be involved in non-bond interactions with Al_2O_3 atoms in the layers of the surface, without increasing the calculation time unreasonably. This structure then converted to have 3D periodicity. As 3D periodic boundary conditions are used, it is important that the size of the vacuum slab is great enough (50 Å) that the non-bond calculations for the adsorbate does not interact with the periodic image of the bottom layer of atoms in the surface.

After minimizing the Al_2O_3 (1 1 1) surface and thiosemicarbazone derivatives molecules, the corrosion system will be built by layer builder to place the inhibitor molecules on Al_2O_3 (1 1 1) surface, and the behaviours of these molecules on the Al_2O_3 (1 1 1) surface were simulated using the COMPASS (condensed phase optimized molecular potentials for atomistic simulation studies) force field.

The Discover molecular dynamics module in Materials Studio 5.0 software from Accelrys Inc. [27] allows selecting a thermodynamic ensemble and the associated parameters, defining simulation time, temperature and pressuring and initiating a dynamics calculation. The molecular dynamics simulations procedures have been described elsewhere [28]. The interaction energy, $E_{\text{Al-inhibitor}}$, of the Al_2O_3 (1 1 1) surface with thiosemicarbazone and its derivatives was calculated according to the following equation:

$$E_{\text{Al-inhibitor}} = E_{\text{complex}} - (E_{\text{Al-surface}} + E_{\text{inhibitor}}) \quad (1)$$

where E_{complex} is the total energy of the Al_2O_3 (1 1 1) surface together with the adsorbed inhibitor molecule, $E_{\text{Al-surface}}$ and $E_{\text{inhibitor}}$ are the total energy of the Al_2O_3 (1 1 1) surface and free inhibitor molecule, respectively. The binding energy between thiosemicarbazone derivatives and Al_2O_3 (1 1 1) surfaces were the negative value of the interaction energy [29], as follow:

$$E_{\text{binding}} = -E_{\text{Al-inhibitor}} \quad (2)$$

4. Results and discussion

4.1. Experimental measurements

4.1.1. Impedance measurements

Impedance spectra for aluminum in 1.0 M HNO_3 solutions, without and in the presence of different concentrations of thiosemicarbazone derivatives, were similar in shape. The shape of the impedance diagrams of aluminum in acidic solution is similar to those found in the literature [30,31]. The presence of thiosemicarbazone derivatives increases the impedance but does not change the other aspects of corrosion mechanism occurred due to their addition. The Nyquist plots presented in Fig. 1 are characterized by three time constants, namely: (1) a capacitive time constant at high frequency values, (2) an inductive time constant at medium frequencies and (3) a second capacitive time constant at low frequencies. In the literature there is no consensus about the origin of the time constants of the impedance diagram. The time constant at high frequencies is attributed to the formation of the oxide layer or to the oxide layer itself. Brett [30] attributed the first capacitance time constant to the interfacial reactions, in particular to the reaction of aluminum oxidation at the metal/oxide/electrolyte interface. The process includes the formation of Al^+ ions at the metal/oxide interface, and their migration through the oxide layer due to high electric field strength, to the oxide/solution interface where they become oxidized to Al^{3+}. The fact that all these processes are represented by only one time constant could be understood either by overlapping of the time constants of separate processes, or by the assumption that one process dominates and, therefore, excludes the other processes [31]. The other possible explanation for the high frequency capacitive constant is the oxide film itself. This assumption was supported by a linear relationship between the inverse of the capacitance and the potential found by Bessone et al. [32]. At the oxide/solution interface where also O^{2-} or OH^- is formed. Simultaneously with the formation of O^{2-} ions, H^+ ions are formed. This results in a local acidification at the oxide–electrolyte interface. The inductive time constant at medium frequencies often attributed to surface or bulk relaxation of species in the oxide film [33].

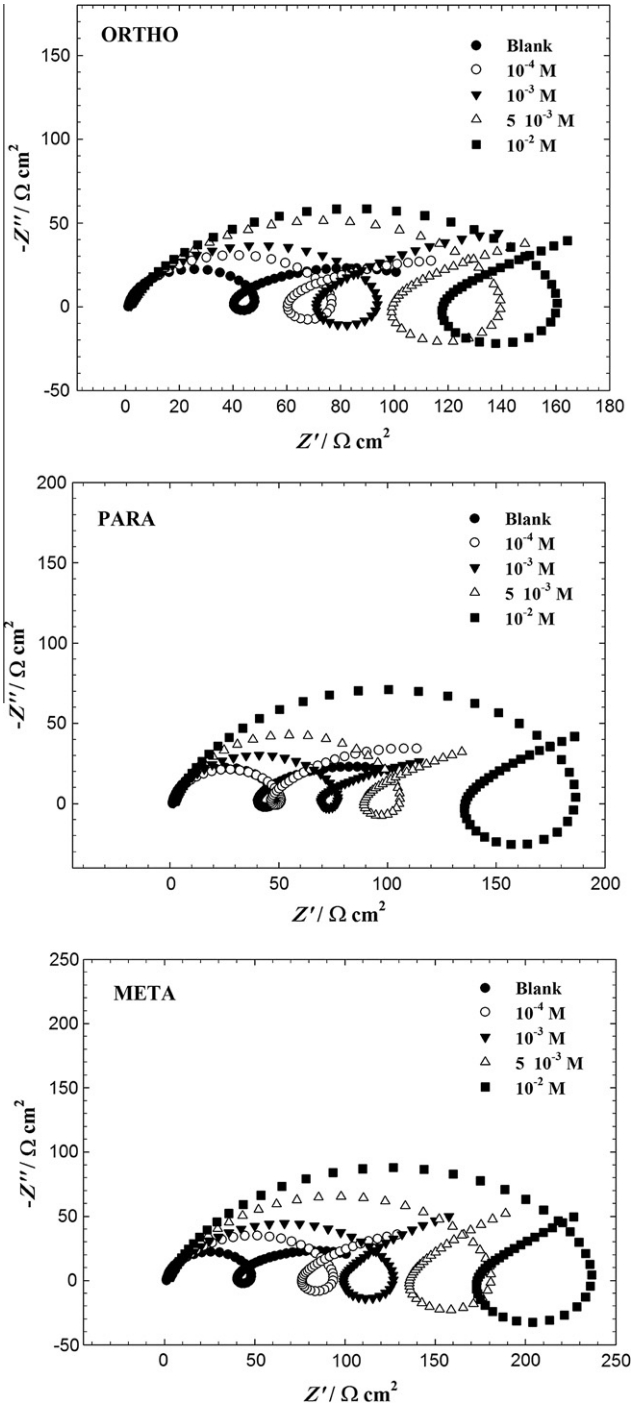

Fig. 1. Niquest plots for aluminum in 1.0 M HNO_3 solutions in the absence and presence of various concentrations of thiosemicarbazone derivatives at 25 ± 1 °C.

The origin of the inductive loop on aluminum is also not clear. It is often attributed to surface or bulk relaxation of species in the oxide layer [33]. Burstein's measurements [34,35] confirmed that the inductive loop is closely related to the existence of a passive film on aluminum. Bessone et al. [32] suggested that the inductive time constant is the result of a rearrangement of surface charge at the metal/oxide interface. It was also proposed that adsorbed intermediates in reduction of hydrogen ions could cause an inductive loop [31,36]. Bessone et al. [37] have observed an inductive loop for the pitted active state on aluminum and attributed it to surface area modulation or salt film property modulation. Adsorption of

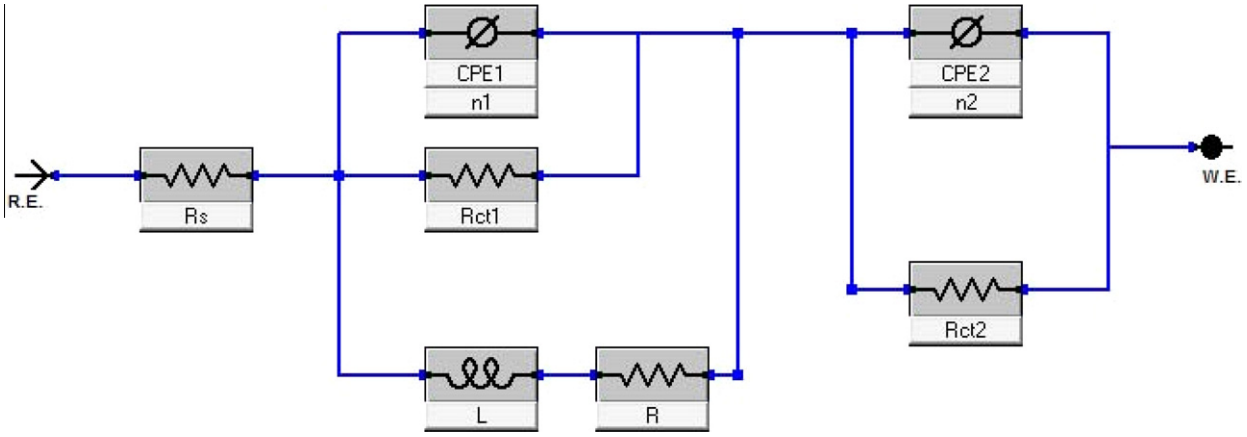

Fig. 2. Equivalent circuit used to model impedance data for aluminum in 1.0 M HNO_3 solutions in the absence and presence of various concentrations of thiosemicarbazone derivatives.

intermediates which in our case are OH^- and NO_2^- ions also causes an inductive loop.

The equivalent circuit used to fit the experimental data of aluminum in 1.0 M HNO_3 solutions without and with different concentrations of thiosemicarbazone derivatives is shown in Fig. 2. The model includes the solution resistance, R_s, a series combination of resistance, R and inductance, L, in parallel with charge-transfer resistance $(R_{ct})_1$, and the constant phase element (CPE_1). In the high frequency limit, the inductive contribution to the overall impedance is insignificant. Therefore, Nyquist plot of the impedance is a semicircle characteristic of the parallel arrangement of the double layer capacitance and charge-transfer resistance corresponding to the aluminum dissolution reaction. Contribution to the total impedance at intermediate frequencies comes mainly from the charge-transfer resistance and inductive component in parallel. The inductor arises from adsorption effects of the oxide film and/or thiosemicarbazone derivatives and could be define as ($L = R\tau$) where τ is the relaxation time for adsorption on aluminum surface. The low frequency locus displays the characteristics of parallel RC circuit. This circuit includes another constant phase element (CPE_2) which is placed in parallel to charge-transfer resistance element $(R_{ct})_2$. The $(R_{ct})_2$ value is a measure of charge-transfer resistance corresponds to the $Al^+ \rightarrow Al^{3+}$ reaction.

The CPE is used in this model to compensate for non-homogeneity in the system and is defined by two values, Q and n. The impedance of CPE is represent by

$$Z_{CPE} = Q^{-1}(j\omega)^{-n} \quad (3)$$

where $j = (-1)^{1/2}$, ω is frequency in rad s^{-1}, $\omega = 2\pi f$ and f is the frequency in Hz. If n equals one, the impedance of CPE is identical to that of a capacitor, $Z_C = (i\omega C)^{-n}$, and in this case Q gives a pure capacitance (C). For non-homogeneous system, n values range from 0.9–1.

Computer fitting of the spectrum allows evolution of the elements of the circuit analogue. The aim of the fitting procedure is to find those values of the parameters which best describe the data, i.e., the fitting model must be consistent with the experimental data. The numerical values of the fitting parameters including polarization resistance $R_p = (R_{ct})_1 + (R_{ct})_2$ are presented in Table 1 and were determined by analysis of the complex plane impedance plots and the equivalent circuit model by means of a computer program (Echem Analyst 5.58 from Gamry).

The experimental data were found to be sufficiently well fitted by the transfer function of the equivalent circuit presented in Fig. 2 within the limits of experimental error and reproducibility of the data. Table 1 shows the impedance parameters recorded for aluminum in 1.0 M HNO_3 solution in absence and presence of various concentrations of the three thiosemicarbazone derivatives at 25 ± 1 °C. The values of the polarization resistance, R_p, increase with increase in concentrations of thiosemicarbazone derivatives showing that the inhibition efficiency of these molecules increases as their concentration increases. Since R_p is inversely proportional to the corrosion rate, it can be used to calculate the inhibition efficiency. The inhibition efficiency obtained from impedance measurements are calculated using Eq. (4).

Table 1
Electrochemical parameters calculated from EIS measurements on aluminum electrode in 1.0 M HNO_3 solutions without and with various concentrations of thiosemicarbazone derivatives at 25 ± 1 °C using equivalent circuit presented in Fig. 2.

	Conc. (M)	R_s (Ω cm²)	Q_1 (Ω^{-1} cm^{-2} S^n)	n_1	$(R_{ct})_1$ (Ω cm²)	L (H cm²)	R (Ω cm²)	Q_2 (Ω^{-1} cm^{-2} S^n)	n_2	$(R_{ct})_2$ (Ω cm²)	R_p (Ω cm²)	λ_z%
	Blank	1.1	30×10^{-6}	0.95	47	3	100	25×10^{-3}	0.55	100	147.0	
ORTHO	10^{-4}	1.3	27×10^{-6}	0.89	50	7	200	35×10^{-3}	0.6	135	185.0	20.5
	10^{-3}	1.5	25×10^{-6}	0.85	75	10	250	36×10^{-3}	0.4	195	270.0	45.5
	5×10^{-3}	1.8	21×10^{-6}	0.56	105	15	290	41×10^{-3}	0.42	297	402.0	63.4
	10^{-2}	1.6	17×10^{-6}	0.8	195	17	350	45×10^{-3}	0.5	305	500.0	70.6
PARA	10^{-4}	1.3	29×10^{-6}	0.85	76	6	130	30×10^{-3}	0.45	152	228.0	35.5
	10^{-3}	1.9	26×10^{-6}	0.83	95	8	169	34×10^{-3}	0.54	208	303.1	51.5
	5×10^{-3}	1.7	21×10^{-6}	0.79	142	15	215	39×10^{-3}	0.45	304	446.1	67.1
	10^{-2}	1.3	18×10^{-6}	0.78	165	16	290	42×10^{-3}	0.42	710	875.1	83.2
META	10^{-4}	1.2	23×10^{-6}	0.799	96	9	250	46×10^{-3}	0.55	168	264.0	44.3
	10^{-3}	1.3	17×10^{-6}	0.76	131	12	320	50×10^{-3}	0.6	241	372.0	60.5
	5×10^{-3}	1.5	15×10^{-6}	0.77	189	17	400	53×10^{-3}	0.58	338	526.8	72.1
	10^{-2}	1.9	10×10^{-6}	0.79	245	20	463	35×10^{-3}	0.45	1022	1267.0	88.4

$$\lambda_z\% = \left(1 - \frac{R_p^o}{R_p}\right) \times 100 \quad (4)$$

where R_p^o and R_p are the polarization resistances for uninhibited and inhibited solutions, respectively. The highest inhibition efficiency was always observed in the presence of META derivatives, somewhat lower in the presence of PARA and ORTHO derivatives. Inspection of Table 1 shows that R_p and double layer capacitance C_{dl} modeled as Q_1, have opposite trend at the whole concentration range. It can be supposed that a protective layer covers the surface of the electrode. Its nature can be some solid film, inhibiting species or both. The decrease in this capacitance Q_1 with increase in thiosemicarbazone derivatives concentrations may be attributed to the formation of a protective layer on the electrode surface [38]. The thickness of this protective layer increases with increase in inhibitor concentration, since more inhibitor molecules electrostatically adsorb on the electrode surface, resulting in a noticeable decrease in Q_1. This trend is in accordance with Helmholtz model, given by Eq. (5) [39]:

$$C_{dl} = \frac{\varepsilon\varepsilon_o A}{d} \quad (5)$$

where d is the thickness of the protective layer, ε is the dielectric constant of the medium, ε_o is the vacuum permittivity and A is the effective surface area of the electrode.

This behaviour confirms the adsorption action of thiosemicarbazone derivatives against aluminum corrosion [40].

4.1.2. Tafel polarization measurements

The polarization behaviour of aluminum electrode in 1.0 M HNO_3 solutions in the absence and presence of different concentrations of thiosemicarbazone derivatives at a scan rate of 1.0 mV s^{-1} and at 25 ± 1 °C is shown in Fig. 3.

These polarization curves demonstrate, as a first sight, that in presence of thiosemicarbazone derivatives the cathodic and anodic branches of the polarization curves are shifted towards lower currents to similar extent, probably as a consequence of the blocking effect of the adsorbed inhibitor molecules. The observed decrease in cathodic and anodic currents was the greatest for META derivative. As it can be seen from Fig. 3, the anodic and cathodic reactions are affected by the thiosemicarbazone derivatives. Based on this result, thiosemicarbazone derivatives inhibit corrosion by controlling both anodic and cathodic reactions (mixed-type inhibitors). Meaning that the addition of thiosemicarbazone derivatives reduces the anodic dissolution of aluminum and also retards the cathodic reactions.

In presence of nitric acid solutions, the reduction reactions involved in the cathodic process is as follow [12]:

$$NO_3^- + 3H^+ + 2e^- \rightarrow HNO_2 + H_2O \quad (6)$$

$$NO_3^- + 4H^+ + 3e^- \rightarrow NO + 2H_2O \quad (7)$$

$$2H^+ + 2e^- \rightarrow H_2 \quad (8)$$

It is clear from Fig. 3 that the cathodic current density is not dominated by oxygen reduction. This is for two reasons; first, they are too high for oxygen reduction. Secondly, they are potential dependent. It would expect reduction of oxygen at these potentials to be diffusion controlled, and therefore independent of potential. Thus, the cathodic reactions are hydrogen evolution and nitrate reduction, Eqs. (6)–(8). Thus the reduction of oxygen can be neglected [41,42].

The generation of polarization curves continues to be important in aqueous corrosion research. Extrapolation of Tafel lines is one of the most popular dc techniques for estimation of corrosion rate.

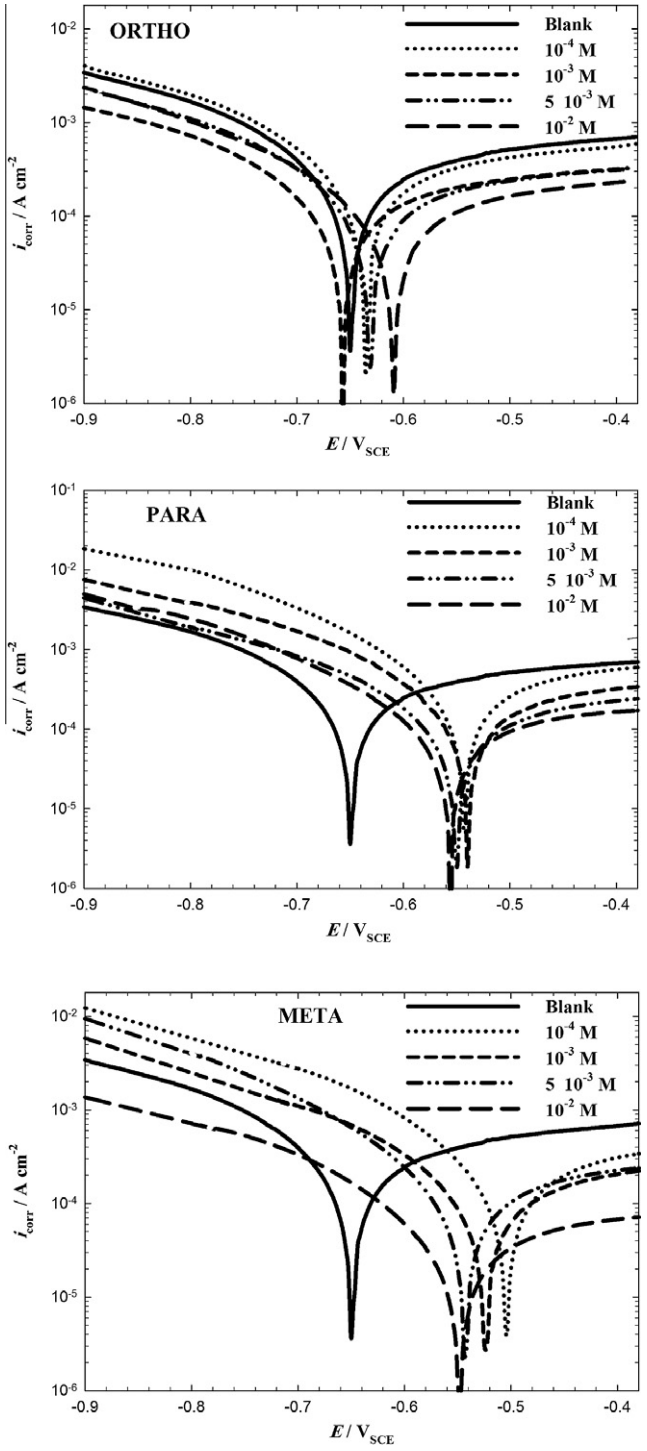

Fig. 3. Anodic and cathodic polarization curves for aluminum in 1.0 M HNO_3 solutions in the absence and presence of various concentrations of thiosemicarbazone derivatives at 25 ± 1 °C.

The extrapolation of anodic and/or cathodic Tafel lines for charge transfer controlled reactions gives the corrosion current density, i_{corr}, at the corrosion potential, E_{corr}. Two rules of thumb should be applied when using Tafel extrapolation. For an accurate extrapolation, at least one of the branches of the polarization curve should exhibit Tafel (i.e., linear on semilogarithmic scale) over at least one decade of current density. In addition, the extrapolation should start at least 50–100 mV away from E_{corr}. These two rules improve the accuracy of manual extrapolations [43].

Inspection of polarization curves in Fig. 3 shows that, it was not possible to evaluate the cathodic or anodic Tafel slopes as there is no visible linear region that prevents linear extrapolation to E_{corr} of the cathodic or anodic polarization curves. The curvature of the anodic polarization curves may be attributed to passivation and pitting [44]. With respect to the cathodic branch, it displays a limiting diffusion current due to the reduction reactions. Thus, the cathodic process is controlled, by concentration polarization rather than activation polarization, which prevented linear extrapolation of the cathodic curves.

As the situation here is more confused and complicated, it is inaccurate to calculate the electrochemical kinetic parameters from Fig. 3 using commercial softwares.

It follows from Fig. 3 that the shapes of the polarization plots for inhibited electrodes are not substantially different from those of uninhibited electrodes. The presence of each inhibitor decreases the corrosion rate but does not change other aspects of the behaviour. This means that the inhibitor does not alter the electrochemical reactions responsible for corrosion. The inhibitive action of these three thiosemicarbazone derivatives therefore may be related to their adsorption and formation of a barrier film on the electrode surface, protecting it from corrosion.

For these reasons we used, as will be seen in the next section, the most accurate and precise method which is weight loss (i.e., non-electrochemical). This is because the experimentation is easy to replicate and, although long exposure times may be involved, the relatively simple procedure reduces the propensity to introduce systematic errors [45].

4.1.3. Weight loss measurements

The percentage inhibition efficiency of the thiosemicarbazone derivatives at a concentration range (10^{-4}–10^{-2} M) and after an immersion period of 48 h are summarized in Table 2. It is seen from Table 3 that the presence of pyridyl ring in meta position has appreciably improved the inhibition characteristics of the META compound. META is the most effective inhibitor of all thiosemicarbazone derivatives. Corrosion of aluminum in aqueous solution has been reported [46,47] to depend on the concentration of anions in solution. A general mechanism for the dissolution of aluminum would be similar to that reported by Ford et al. [48] as well as Nguyen and Foley [46,49].

$$Al_{(s)} + H_2O \underset{k_2}{\overset{k_1}{\rightleftarrows}} AlOH_{ads} + H^+ + e \quad (9)$$

$$AlOH_{(ads)} + 5H_2O + H^+ \underset{k_{-2}}{\overset{k_2}{\rightleftarrows}} Al^{3+}\cdot 6H_2O + 2e \quad (10)$$

$$Al^{3+} + H_2O \underset{k_{-3}}{\overset{k_3}{\rightleftarrows}} [AlOH]^{2+} + H^+ \quad (11)$$

$$[AlOH]^{2+} + X^{-1} + \underset{k_{-4}}{\overset{k_4}{\rightleftarrows}} [AlOHX]^+ \quad (12)$$

The controlling step in the metal dissolution is the complexation reaction between the hydrated cation and the anion, see Eq. (12). In the presence of nitrate ions the reaction corresponds to

$$[AlOH]^{2+} + NO_3^- + \underset{k_{-4}}{\overset{k_4}{\rightleftarrows}} [AlOHNO_3]^+ \quad (13)$$

The soluble complex ion formed increases the metal dissolution rate which depends on the nitric acid concentration [38].

Fig. 4 shows plots of corrosion rate (expressed in mm y^{-1}) versus thiosemicarbazone derivatives concentration at 25 ± 1 °C. Corrosion rate of aluminum electrode decreases as the concentration of thiosemicarbazone derivatives increases. The various parameters derived from weight loss measurements, regarding the corrosion of aluminum in 1.0 M HNO_3 solutions without and with various concentrations of the three inhibitors are summarized in Table 2. The inhibition efficiencies, $\sigma_w\%$ of the three tested thiosemicarbazone were calculated by using Eq. (14)

$$\sigma_w\% = \left(1 - \frac{\partial_{corr}}{\partial^o_{corr}}\right) \times 100 \quad (14)$$

where ∂^o_{corr} and ∂_{corr} are corrosion rates without and with different concentrations of thiosemicarbazone derivatives, respectively. It is obvious from Fig. 4 and the data presented in Table 2, that the corrosion rate decreases, and the corresponding inhibition efficiency increases as the concentrations of the thiosemicarbazone derivatives increase. This decrease in corrosion rate, and the corresponding increase in efficiency, enhances in the order: ORTH < PARA < META. These findings reflect, as will be seen and

Table 2
Corrosion rate and inhibition efficiency data obtained from weight loss measurements for Al in 1.0 M HNO_3 solutions in absence and presence of various concentrations of thiosemicarbazone derivatives 3 at 25±1 °C.

Inhibitor	Conc. (M)	Corrosion rate/ mg cm^{-2} h^{-1}, ∂	Corrosion rate/ mm y^{-1}	$\sigma_w\%$
	Blank	0.451	5.01	–
ORTHO	10^{-4}	0.35	3.8	22.4
	10^{-3}	0.25	2.7	44.5
	5×10^{-3}	0.18	2.0	60.1
	10^{-2}	0.13	1.4	71.2
PARA	10^{-4}	0.31	3.4	31.3
	10^{-3}	0.23	2.5	49.0
	5×10^{-3}	0.16	1.7	64.5
	10^{-2}	0.09	1.0	80.1
META	10^{-4}	0.26	2.8	42.4
	10^{-3}	0.17	1.8	62.3
	5×10^{-3}	0.11	1.2	75.6
	10^{-2}	0.04	0.44	91.2

Table 3
Some parameters from Langmuir isotherm model for aluminum in 1.0 M HNO_3.

Inhibitor	Langmuir			
	ΔG^o_{ads} (kJ/mol)	Slope	K_{ads} (dm^3 mol^{-1})	R^2
ORTHO	−27.7	1.36	1290.6	0.99
PARA	−27.8	1.22	1360.1	0.98
META	−28.7	1.08	1989.0	0.99

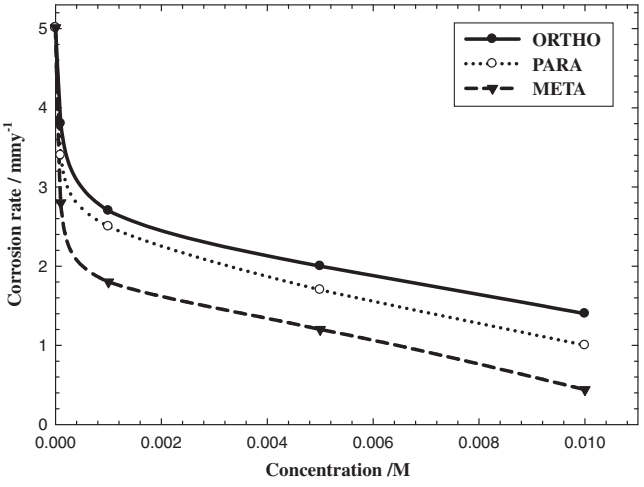

Fig. 4. Dependence of corrosion rates of the three thiosemicarbazone derivatives on their concentrations at 25 ± 1 °C.

fully discussed, the highest inhibition performance of META as compared with ORTH and PARA. These selected thiosemicarbazones, therefore inhibit aluminum corrosion in 1.0 M HNO_3 to an extent depending on inhibitor concentration and its type.

It is worth noting from Tables 1 and 2 that the inhibition efficiency values obtained from weight loss and electrochemical measurements are comparable and run parallel with each other. The little difference found in results obtained from both chemical and electrochemical measurements were also reported previously [50]. They attributed this difference between electrochemically and chemically determined corrosion rates to the operation of a separate potential independent of chemical dissolution process which co-exists with the electrochemical process.

4.2. Adsorption considerations

A direct relationship between inhibition efficiency ($\sigma_w\%$) and the degree of surface coverage (θ) [$\sigma_w\% = 100 \times \theta$] can be assumed for the different concentrations of the inhibitor. The degree of surface coverage (θ) for the different concentrations of thiosemicarbazone derivatives has been evaluated from the weight loss measurements in 1.0 M HNO_3 at 25 ± 1 °C. The data were tested graphically by fitting to various adsorption isotherms including Freundlich, Temkin, Flory–Huggins, Bockris–Swinkles, Langmuir and Frumkin isotherms. The correlation coefficient (R^2) was used to determine the best fit isotherm which was obtained for Langmuir. According to this isotherm, θ is related to the inhibitor concentration by the following Eq. (15) [51].

$$\frac{C}{\theta} = \frac{1}{K_{ads}} + C \tag{15}$$

where θ is the surface coverage, C is the concentration, K_{ads} is the equilibrium constant of adsorption process. K_{ads} is related to the standard Gibbs free energy of adsorption ΔG^o_{ads} by the Eq. (16) [52].

The data was obtained from Fig. 5. The intercept of the lines in Fig. 5 yielded K_{ads} in ($dm^3\ mol^{-1}$), and the corresponding standard Gibbs free energy of adsorption in (kJ mol^{-1}) was then calculated from Eq. (16) [52]:

$$K_{asd} = \frac{1}{C_{solvent}} \exp\left(\frac{-\Delta G^o_{ads}}{RT}\right) \tag{16}$$

where R in (J mol^{-1} K^{-1}) is the gas constant, T (K) is the temperature, and $C_{solvent}$ is the molar concentration of the solvent, which in this case, is water ($C_{H_2O} = 55.5$ mol dm^{-3}). Using this equation, the various adsorption parameters are obtained from the studied isotherm including the standard Gibbs free energy of adsorption of thiosemicarbazone derivatives on the aluminum surface at 295 K was calculated and listed in Table 3.

Fig. 5 shows the plot of C/θ versus C and linear plots were obtained for the different thiosemicarbazone derivatives indicating that the adsorption of these inhibitors followed Langmuir isotherm. The various adsorption parameters obtained from this isotherm are listed in Table 3. It is seen from Table 3 that the correlation coefficients are very good and K_{ads} values increases with increasing inhibitor concentration showing that the molecules of the inhibitors were adsorbed on the aluminum surface. Although the plots are linear as depicted by R^2 values (0.99) however, the slopes deviates from the value of unity as expected from the ideal Langmuir adsorption equation. This deviation may be explained on the basis of the interaction among adsorbed species on the surface of the metal. It has been postulated in the derivation of Langmuir isotherm equation that adsorbed molecules do not interact with one another, but this is not true in the case of large organic molecules having polar atoms or groups which can adsorbed on the cathodic and anodic sites of the metal surface. Such adsorbed species interact by mutual repulsion or attraction. It is also possible that the inhibitors studied can be adsorbed on the anodic and cathodic sites resulting in deviation from unit gradient. Similar observation has been reported in the literature [53,54].

Results presented in the Table 3, indicate that the values of ΔG^o_{ads} are negative and lies between −27.7 and 28.7 kJ mol^{-1}. The negative values signify adsorption of the inhibitor molecules via mixed adsorption mechanism. It is also seen that the values of ΔG^o_{ads} increased with an increase in inhibitor concentrations, a phenomenon which indicates that the adsorption of the inhibitor onto aluminum surface was favorable with increasing thiosemicarbazone derivatives concentrations.

Literature demonstrates that the values of standard Gibbs free energy of adsorption in aqueous solution around −20 kJ mol^{-1} or lower (more positive) indicate adsorption with electrostatic interaction between the adsorbent and adsorbate (physisorption), while those around or higher (more negative) than −40 kJ mol^{-1} involve

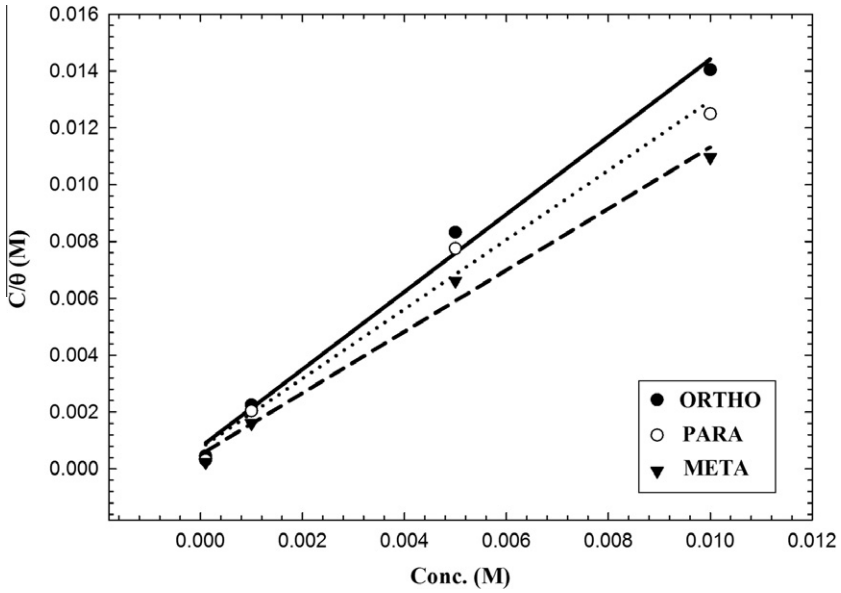

Fig. 5. Langmuir adsorption isotherm model for aluminum in 1.0 M HNO_3 containing thiosemicarbazone derivatives at 25 ± 1 °C.

charge sharing between the molecules and the metal (chemisorption) [55]. However, this should be taken with caution since the enthalpy of adsorption is the parameter that actually reflects the adsorption bond strength, rather than the standard Gibbs free energy of adsorption [52].

Physisorption is consistent with electrostatic interaction between charged molecules and a charged aluminum surface while chemisorption is consistent with charge sharing or charge transfer from the inhibitor components to the metal surface to form a coordinate type of bond.

4.3. Computational study

The researchers are often encouraged to use theoretical data in their studies not only to support their experimental results but also to find the efficient way to minimize the chemical expenditures. Therefore, recently more corrosion publications contain substantial quantum chemical calculations [56].

According to the frontier molecular orbital theory, the formation of a transition state is due to an interaction between frontier orbitals (HOMO and LUMO) of reacting species [57]. Thus, the treatment of the frontier molecular orbitals separately from the other orbitals is based on the general principles governing the nature of chemical reactions. The effectiveness of an inhibitor can be related with its electronic and spatial molecular structure. Certain quantum-chemical parameters that can be related to the interactions of metal-inhibitor, these are: the HOMO energy that is often associated with the capacity of a molecule to donate electrons, the energy gap ΔE (the lower values of energy gap, the better corrosion inhibition), and the dipole moment μ, because low values will favor the accumulation of inhibitor molecules on the metallic surface. A good correlation between the rate of corrosion and E_{HOMO}, as well as with energy gap ($\Delta E = E_{LUMO} - E_{HOMO}$) has been found in previous works [58,59].

Fig. 6 shows the optimization energies of the studied thiosemicarbazone derivatives. As can be seen in Fig. 6 the lowest energy is calculated for the META derivatives, PARA and ORTHO, respectively.

In Table 4, several quantum-chemical parameters calculated by using DFT method.

Table 4
HOMO and LUMO energies, HOMO–LUMO gap (ΔE) and dipole moment μ for ORTHO, PARA and META obtained using DFT calculations.

Inhibitor	E_{HOMO} (kJ mol^{-1})	E_{LUMO} (kJ mol^{-1})	$\Delta E = E_{LUMO} - E_{HOMO}$ (kJ mol^{-1})	μ/ (D)	σ_w%
ORTHO	−867.4	73.3	940.7	6.2	71.2
PARA	−792.2	50.3	842.4	5.2	80.1
META	−760.3	33.8	794.2	4.52	91.2

The HOMO energy can indicate the disposition of the molecule to donate electrons to an appropriated acceptor with empty molecular orbitals (p orbital in aluminum). Also, an increase in the values of E_{HOMO} can facilitate the adsorption, and therefore improved inhibition efficiency results [60]. The corrosion rate decreases with increases in HOMO energy (less negative) [58], therefore an increase in the corrosion inhibition is present (see Table 4). Low values of the energy gap (ΔE) will provide good inhibition efficiencies, because the excitation energy to remove an electron from the last occupied orbital will be low [61]. The results show that the META derivative has the lowest energy gap; this agrees with the experimental results which indicate that this molecule could have better performance as a corrosion inhibitor. For the thiosemicarbazone derivatives the nature of their molecular orbitals, HOMO (highest occupied molecular orbital) and LUMO (lowest unoccupied molecular orbital) are presented in Fig. 7.

It is well known in the literature that the sulphur atom of the thio-compounds is the reaction center for adsorption onto a metal surface [62]. The HOMO location in the thiosemicarbazone derivatives are mostly distributed in the thio group as well as the amino group, see Fig. 7, indicating that the preferred sites for the electrophilic attack through metallic cations are located on the nitrogen and sulphur atoms. It is probably that the parts of the molecules with high HOMO density were oriented towards the aluminum oxide surface and the adsorption of these ones could be sharing the lone pair of electrons for nitrogen atoms and the π-electrons of the aromatic ring [63]. Therefore the electron density on this atom would determine the effectiveness of this type of inhibitors. In thiosemicarbazone derivatives, the electron density of the nitrogen and sulphur atoms is localized around these atoms. Substitution of pyridyl group for hydrogen leads to the withdrawal of

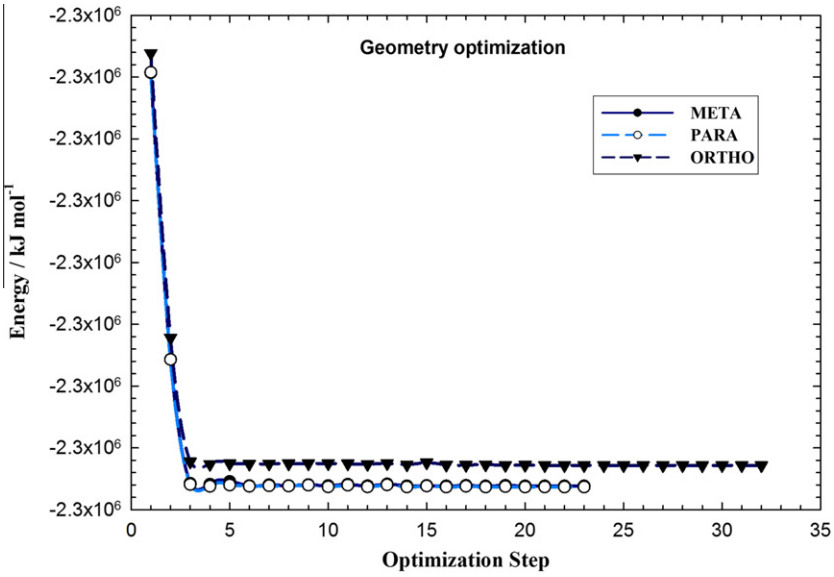

Fig. 6. Optimization energy for thiosemicarbazone derivatives obtained by DFT method.

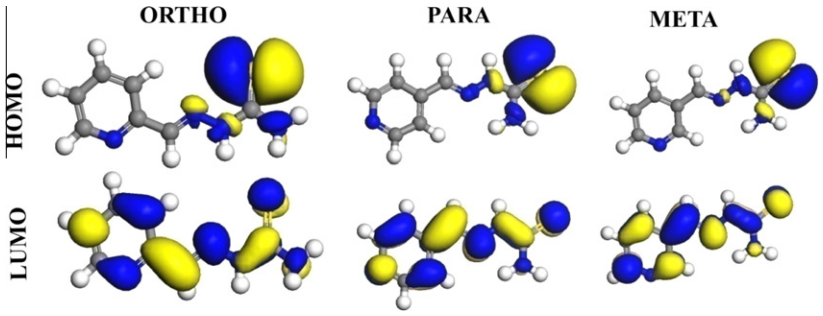

Fig. 7. Molecular orbital plots for thiosemicarbazone derivatives.

electrons from these atoms and tends to delocalize the charges throughout pyridyl ring and lowers the basicity [64].

Furthermore, in order to confirm the adsorption sites of thiosemicarbazone derivatives molecules when adsorbed on Al_2O_3 surface via chemical bond, the local reactivity of these molecules were investigated by analysis of their Fukui indices [65]. Since they indicate the reactive regions, in the form of the nucleophilic and electrophilic behaviour of each atom in the molecule.

The FI calculations were performed with Dmol^3 software using Mulliken population analysis [66] or a numerical integration procedure such as a Hirshfeld analysis [67]. The $f^+(r)$ measures the density of changes when the molecule gains electrons and it corresponds to reactivity with respect to nucleophilic attack. On the other hand, $f^-(r)$ corresponds to reactivity with respect to electrophilic attack or when the molecule losses electrons.

The Fukui function $f(r)$ is defined as the first derivative of the electronic density $\rho(r)$ with respect to the number of electrons N at a constant external potential $v(r)$. Thus using a scheme of finite differences, we had [68]:

$$f^+(r) = \rho_{N+1}(r) - \rho_N(r)(\text{for nucleophilic attack}) \quad (17)$$

$$f^-(r) = \rho_N(r) - \rho_{N-1}(r)(\text{for electrophilic attack}) \quad (18)$$

where ρ_{N+1}, ρ_N and ρ_{N-1} are the electronic densities of anionic, neutral and cationic species, respectively.

The N corresponds to the number of electrons in the molecule. $N+1$ corresponds to an anion, with an electron added to the LUMO of the neutral molecule. $N-1$ correspondingly is the cation with an electron removed from the HOMO of the neutral molecule. All calculations are done at the ground-state geometry. These functions can be condensed to the nuclei by using an atomic charge partitioning scheme.

Table 5
Calculated Mulliken atomic charges and Fukui functions for the three selected thiosemicarbazone derivatives.

	Atom	q_N	q_{N+1}	q_{N-1}	f_k^+	f_k^-
ORTHO	N(3)	−0.28	−0.24	−0.29	0.04	0.02
	N(8)	−0.05	−0.02	−0.01	0.07	−0.06
	N(9)	−0.22	−0.22	−0.21	0.002	−0.01
	S(11)	−0.49	−0.34	−1.03	0.16	0.53
	N(12)	−0.43	−0.40	−0.44	0.03	0.02
PARA	N(3)	−0.56	−0.38	−0.59	0.17	0.04
	N(8)	−0.14	0.04	−0.02	0.18	−0.12
	N(9)	−0.38	−0.27	−0.24	0.11	−0.13
	S(11)	−0.52	−0.22	−1.05	0.29	0.53
	N(12)	−0.31	−0.19	−0.33	0.12	0.02
META	N(2)	−0.24	0.04	0.08	0.28	−0.32
	N(3)	−0.48	−0.2	−0.45	0.28	−0.03
	S(5)	−0.53	0.07	−1.06	0.59	0.53
	N(6)	−0.41	−0.18	−0.53	0.22	0.12
	N(9)	−0.54	−0.31	−0.66	0.23	0.12

Table 5 shows Mulliken atomic charges calculated for the studied molecules. It is inferred that the more negative the atomic charges of the adsorbed center, the more easily the atom donates its electrons to the unoccupied orbital of the metal. It is clear from Table 5, that nitrogen and sulphur atoms carrying negative charges centers which could offer electrons to the Al_2O_3 surface to form a co-ordinate type of bond.

The values of FI of thiosemicarbazone were displayed in Table 5. It could be seen that the Fukui indices of atoms in these molecules changed when the pyridyl group attached to different positions of thiosemicarbazone, which indicated that the local reactivity of these molecules was sensitive to the point of attachment.

The highest FI values are presented in Table 5 for the heteroatoms only. META has propitious zones for nucleophilic attack located on (N2, N3, S5 and N9) while PARA has only on (N8, S11 and N12). ORTHO has only nucleophilic centers on (S11). Data in Table 5 shows that META has more susceptible sites for adsorption on the aluminum surface in nitric acid.

The interaction of thiosemicarbazone derivatives with the Al_2O_3 (1 1 1) surface was investigated with molecular dynamics (MD) simulation. An adsorption model containing one inhibitor molecule and metallic surface was built using Discover module in Materials Studio 5.0 software. During simulations, all the bulk atoms in the Al_2O_3 (1 1 1) systems were kept "frozen", and the inhibitor molecules were allowed to interact with the metal oxide surface freely. The simulation system was optimized with COMPASS force field [69]. The canonical ensemble MD simulation was performed with Discover module in Materials Studio 5.0. The simulation temperature was set at 298 K, and the temperature was controlled by Andersen thermostat [70]. The initial velocity of each molecule accorded with Maxwell–Boltzmann distribution. Based on hypotheses, such as periodic boundary condition and equivalence of time-average and ensemble-average, Newtonian motion equations were solved with velocity verlet algorithm [71]. Van der Waals and coulomb interactions were calculated by group-based method, and the potential function was given as follows:

$$\Phi = \frac{1}{4\pi\varepsilon}\left[\frac{\psi}{r} + \frac{\mu\cos\alpha}{r^2} + \frac{\Theta(3\cos 2\alpha - 1)}{r^3}\right] \quad (19)$$

Herein, ψ , μ, α and Θ represent total charge, dipole moment, electric quadrupole moment and orientation angle of the group, respectively, and r represents the radial distance of the group center. The cutoff radius was 1.2 nm, and the intermolecular interaction energy beyond cutoff radius was revised with average density approximation. The time step was 1 fs, the simulation time was 1000 ps, and a frame was recorded every 2500 steps during simulation [72].

The values of the interaction energy and the binding energy of the studied thiosemicarbazone derivatives on Al_2O_3 (1 1 1) surface are listed in Table 6. As can be seen from Table 6, the binding energy has a positive value. The higher the binding energy, the more

Table 6
Interaction and binding energies for thiosemicarbazone derivatives adsorbed on Al_2O_3 (1 1 1) calculated using molecular dynamics simulations.

Inhibitor	Interaction energy $E_{Al\text{-}inhibitor}$ (kJ mol^{-1})	Binding energy $E_{binding}$ (kJ mol^{-1})
ORTHO	−651.5	651.5
PARA	−465.3	465.3
META	−326.1	326.1

easily the inhibitor adsorbs on the metal surface, the higher is the inhibition efficiency [73]. Compared to PARA and ORTHO derivatives, META has the highest binding energy to the Al_2O_3 (1 1 1) surface that found during the simulation process. Here again, the high values of binding energy obtained with META explain, in consistence with the experimental findings, its higher inhibition efficiency from the theoretical point of view.

Based on the equilibrium configuration of thiosemicarbazone derivatives adsorbed on Al_2O_3 (1 1 1) surface, Fig. 8, one can draw a conclusion that thiosemicarbazone derivatives adsorb mainly, as will be seen and fully discussed in next section, via the N and S-atoms. In this way, the exposed part of electrode surface can be reduced due to its coverage by the inhibitor molecule via S-atoms, preventing the acid corrosion of aluminum.

4.4. Inhibition mechanism

Adsorption is known to be the key mechanism of inhibition action, and it might be suggested that the inhibitor molecules are adhered to the metal surface, which decreases the surface area at which cathodic and anodic reactions take place. It is generally accepted that organic molecules inhibit corrosion by adsorption at the metal/solution interface and that the adsorption depends on the molecule's chemical composition, the temperature and the electrochemical potential at the metal/solution interface. In case of aluminum surface, the solvent H_2O molecules could also adsorb on the aluminum oxide surface forming hydroxylated sites, or hydroxide layers at the surface (M−OH), that impart a pH-dependent surface charge. The polar hydroxyl (—OH^-) groups may cause the surface to attract and physically adsorb a single or several additional layers of polar water molecules. An oxide or hydroxide surface (Al-OH) becomes charged by reacting with H^+ or OH^- ions due to surface amphoteric reactions as presented in equations:

$$\text{Al-OH} + H^+ \rightleftarrows \text{Al-OH}^{2+} \quad (20)$$

$$\text{Al-OH} + OH^- \rightleftarrows \text{Al-O}^- + H_2O \quad (21)$$

In 1.0 M HNO_3, where pH is low, hydroxide surface adsorbs protons to produce positively charged surfaces (Al-OH_2^+).

The number of these sites and the surface charge of the oxide are determined by the pH of the solution. Surface charge influences adsorption of ions from solution and other interfacial phenomena [74]. The pH of the potential of zero charge (PZC) for aluminum oxides/hydroxides is between 6 and 9, and in acidic solution, the accumulation of Al-OH_2^+ species accounts for the surface charge [75,76].

In acidic solution, therefore the positively charged surface sites will electrostatically attract any anions present in solution, and repel cations.

Thiosemicarbazone derivatives may adsorbed on the aluminum oxide surface in four different adsorption types: (a) electrostatic interaction between a negatively charged surface, which is provided with specifically adsorbed anions (NO_3^-, NO_2^-) on aluminum and the positive charge of the inhibitor (in case of protonation of the inhibitor), (b) interaction of unshared electron pairs in the molecule (present in sulphur and/or nitrogen) with the aluminum surface, (c) interaction of π-electron of the pyridyl rings with aluminum surface and (d) a combination of the (a–c) types. Efficient adsorption is the result of either π-electron of the thiosemicarbazone system or the electronegative N and S (hetro-atom) atoms [77].

The chemical adsorption is probably the most important type of interaction between the Al_2O_3 surface and the thiosemicarbazone derivatives. Here, the adsorbed species are in contact with the Al_2O_3 surface. In this process, a coordinated bond that involves the electron transfer from inhibitor system towards the metallic surface is formed.

The electron-transfer is facilitated when the inhibitor molecule has a lone pair of electrons without share in the donating atom of the functional group, and the availability of π-electrons due to the presence of double bonds or aromatic rings in its structure.

Moreover, there is a great possibility that adsorption may also take place via hydrogen bond formation between the N–H linkage in thiosemicarbazone derivatives and the oxygen atoms of the aluminum oxide/aluminum hydroxide surface species. This type of adsorption should be more prevalent for protonated N-atoms, because the positive charge on the N-atom is conductive to the formation of hydrogen bonds. Unprotonated N-atoms may adsorb by direct chemisorption, as mentioned previously, or by hydrogen bonding to a surface oxidized species. The extent of adsorption by the respective modes depends on the nature of the metal surface. A good inhibitor must have strong affinity for the bare metal atoms. The requirement is different in case of aluminum; a compact passive oxide film is always present on the electrode surface, where hydrogen bond formation accounts for most of the inhibition ac-

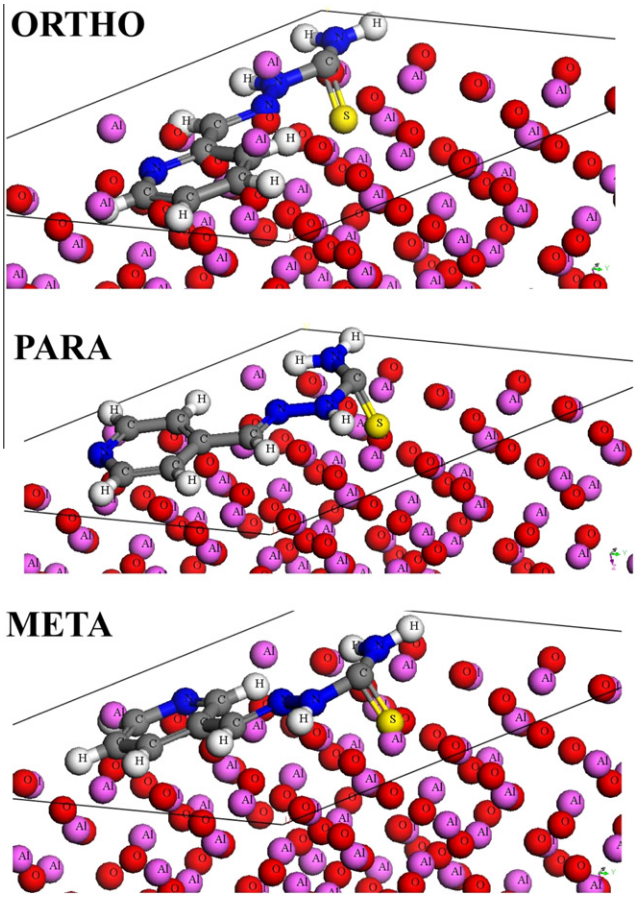

Fig. 8. Modes of adsorption of META, PARA and ORTHO on Al_2O_3 surface (1 1 1).

tion. An effective inhibitor is one that forms hydrogen bonds easily with the oxidized surface.

5. Conclusion

Chemical and electrochemical measurements incorporated with quantum chemical calculations and molecular dynamics simulations were used to study the corrosion inhibition characteristics of some thiosemicarbazone derivatives on aluminum in 1.0 M HNO_3 solutions. The results obtained lead to the conclusion that thiosemicarbazone derivatives effectively inhibit the corrosion of aluminum in 1.0 M HNO_3 solutions. The inhibition efficiency of these compounds increases with increase in their concentrations. Polarization curves demonstrated that the thiosemicarbazone derivatives were of mixed-type inhibitors for A_2O_3 (1 1 1) surface corrosion in these solutions. EIS plots indicated that the addition of inhibitors increases the charge-transfer resistance of the corrosion process, and hence the inhibition performance, enhances with inhibitor concentration and depends on the type of the adsorbed molecule.

The molecular dynamics simulation results show that the three thiosemicarbazone derivatives can adsorb on the A_2O_3 (1 1 1) surface through the sulphur and nitrogen atoms as well as π-electrons in the pyridyl structure. Physisorption, followed by chemisorption is proposed as the mechanism for the inhibition process which is enhanced via formation of hydrogen bonding.

References

[1] D.D.N. Singh, M.M. Singh, R.S. Chaudhary, C.V. Agarwal, Inhibition and polarization studies of some substituted urea compounds for corrosion of aluminum in nitric acid, Electrochim. Acta 26 (1981) 1051–1056.
[2] R.B. Mears, G.G. Eldredge, Ind. Eng. Chem. 37 (1945) 736–743.
[3] D.D.N. Singh, R.S. Chaudhary, B. Prakash, C.V. Agrawal, Inhibitive efficiency of some substituted thioureas for the corrosion of aluminum in nitric acid, Br. Corros. J. 14 (1979) 235–239.
[4] D.D.N. Singh, R.S. Chaudhary, C.V. Agrawal, A thio-urea based inhibitor for the corrosion of aluminium in nitric acid, J. Electrochem. Soc. India 28 (1979) 241–249.
[5] R.S. Chaudhary, D.D.N. Singh, C.V. Agrawal, Inhibitive action of some para substituted aromatic amines towards corrosion of aluminium in nitric acid solution, J. Electrochem. Soc. India 27 (1978) 91–99.
[6] D.D.N. Singh, R.S. Choudhary, C.V. Agrawal, Corrosion characteristics of some aluminium alloys in nitric acid, J. Electrochem. Soc. 129 (1979) 1982–1991.
[7] S. Floate, M.G. Hosseini, M.R. Arshadi, D. Ritson, K.L. Young, R.J. Nichols, An in-situ infrared spectroscopic study of the adsorption of citrate on Au(1 1 1) electrodes, J. Electroanal. Chem. 542 (2003) 67–74.
[8] W.R. Fawcett, R.J. Forster, M.R. Philpott, M.J. Weaver, S.A. Wasileski, L. Coury, J. Leddy, Recent developments in double layer studies, Interface 94 (2000) 22–24.
[9] K.F. Khaled, M. Amin, Corrosion monitoring of mild steel in sulphuric acid solutions in presence of some thiazole derivatives – molecular dynamics, chemical and electrochemical studies, Corros. Sci. 51 (2009) 1964–1975.
[10] K.F. Khaled, M. Amin, Dry and wet lab studies for some benzotriazole derivatives as possible corrosion inhibitors for copper in 1.0 M HNO_3, Corros. Sci. 51 (2009) 2098–2106.
[11] M. Amin, K.F. Khaled, Q. Mohsen, A. Arida, A study of the inhibition of iron corrosion in HCl solutions by some amino acids, Corros. Sci. 52 (2010) 1684–1695.
[12] K.F. Khaled, Sahar A. Fadl-Allah, B. Hammouti, Some benzotriazole derivatives as corrosion inhibitors for copper in acidic medium: experimental and quantum chemical molecular dynamics approach, Mat. Chem. Phys. 117 (2009) 148–155.
[13] K.F. Khaled, Experimental and atomistic simulation studies of corrosion inhibition of copper by a new benzotriazole derivative in acid medium, Electrochim. Acta 54 (2009) 4345–4352.
[14] K.F. Khaled, Molecular simulation, quantum chemical calculations and electrochemical studies for inhibition of mild steel by triazoles, Electrochim. Acta 53 (2008) 3484–3492.
[15] S. Yuan, S.O. Pehkonen, B. Liang, Y.P. Ting, K.G. Neoh, E.T. Kang, Poly(1-vinylimidazole) formation on copper surfaces via surface-initiated graft polymerization for corrosion protection, Corros. Sci. 52 (2010) 1958–1968.
[16] J. Vosta, J. Eliasek, Study on corrosion inhibition from aspect of quantum chemistry, Corros. Sci. 11 (1971) 223–229.
[17] J. Zhang, J. Liu, W. Yu, Y. Yan, L. You, L. Liu, Molecular modeling of the inhibition mechanism of 1-(2-aminoethyl)-2-alkyl-imidazoline, Corros. Sci. 52 (2010) 2059–2065.
[18] Y. Tang, X. Yang, W. Yang, R. Wan, Y. Chen, X. Yin, A preliminary investigation of corrosion inhibition of mild steel in 0.5 M H_2SO_4 by 2-amino-5-(n-pyridyl)-1,3,4-thiadiazole: polarization, EIS and molecular dynamics simulations, Corros. Sci. 52 (2010) 1801–1808.
[19] N. Soltani, M. Behpour, S.M. Ghoreishi, H. Naeimi, Corrosion inhibition of mild steel in hydrochloric acid solution by some double Schiff bases, Corros. Sci. 52 (2010) 1351–1365.
[20] J.M. Costa, J.M. Lluch, The use of quantum mechanics calculations for the study of corrosion inhibitors, Corros. Sci. 24 (1984) 929–933.
[21] R. Hasanov, S. Bilge, S. Bilgiç, G. Gece, Z. Kılıç, Experimental and theoretical calculations on corrosion inhibition of steel in 1 M H_2SO_4 by crown type polyethers, Corros. Sci. 52 (2010) 984–990.
[22] I. Lukovits, E. Kalman, I. Baka, I. Felhasi, J. Teledgi, In: Proc. Eighth Eur. Symp. Corros. Inhibitors (8SEIC), vol. 10, Ann. Univ. Ferrara, Italy, 1995, pp. 543–555.
[23] I. Lukovits, T. Kostalanyi, E. Kalman, G. Palinkos, Conference Corrosion 99, San Antonia, TX, USA, 1999, pp. 565–573.
[24] Y. Tang, X. Yang, W. Yang, Y. Chen, R. Wan, Experimental and molecular dynamics studies on corrosion inhibition of mild steel by 2-amino-5-phenyl-1,3,4-thiadiazole, Corros. Sci. 52 (2010) 242–249.
[25] G. Gece, S. Bilgiç, Quantum chemical study of some cyclic nitrogen compounds as corrosion inhibitors of steel in NaCl media, Corros. Sci. 51 (2009) 1876–1878.
[26] G. Bereket, C. Ogretir, E. Hur, Quantum chemical studies on some imidazole derivatives as corrosion inhibitors for iron in acidic medium, J. Mol. Struct. (THEOCHEM) 578 (2001) 79–88.
[27] J. Barriga, B. Coto, B. Fernandez, Tribol. Int. 40 (2007) 960.
[28] K.F. Khaled, Monte Carlo simulations of corrosion inhibition of mild steel in 0.5 M sulphuric acid by some green corrosion inhibitors, J. Solid Stat. Electrochem. 13 (2009) 1743–1756.
[29] T. Mineva, V. Parvanov, I. Petrov, N. Neshev, N. Russo, Fukui indices from perturbed kohn-sham orbitals and regional softness from mayer atomic valences, J. Phys. Chem. A 105 (2001) 1959–1967.
[30] C.M.A. Brett, Studies on aluminum corrosion in hydrochloric acid solution, Portug. Electrochim. Acta 7 (1989) 123–126.
[31] H.J.W. Lenderink, M.V.D. Linden, J.H.W.D.E. Wit, Corrosion of aluminum in acidic and neutral solutions, Electrochim. Acta 38 (1993) 1989–1992.
[32] J.B. Bessone, C. Mayer, K. Jutner, W.J. Lorenz, AC-impedance measurements on aluminum barrier type oxide films, Electrochim. Acta 28 (1983) 171–175.
[33] S.E. Frers, M.M. Stefenel, C. Mayer, T. Chierchie, AC-impedance measurements on aluminium in chloride containing solutions and below the pitting potential, J. Appl. Electrochem. 20 (1990) 996–999.
[34] G.T. Burstein, R.J. Cinderey, The potential of freshly generated metal surfaces determined from the guillotined electrode – a new technique, Corros. Sci. 32 (1991) 1195–1211.
[35] R.J. Cinderey, G.T. Burstein, Evolution of the corrosion potential of repassivating aluminum surfaces, Corros. Sci. 33 (1992) 475–492.
[36] M. Metikoš-Huković, R. Babić, Z. Grubač, Corrosion protection of aluminium in acidic chloride solutions with nontoxic inhibitors, J. Appl. Electrochem. 28 (1998) 433–439.
[37] J.B. Bessone, D.R. Salinas, C. Mayer, M. Ebert, W.J. Lorenz, An EIS study of aluminium barrier-type oxide films formed in different media, Electrochim. Acta 37 (1992) 2283–2290.
[38] E. McCafferty, N. Hackerman, Double layer capacitance of iron and corrosion inhibition with polymethylene diamines, J. Electrochem. Soc. 119 (1972) 146–154.
[39] C. Bataillon, S. Brunet, Electrochemical impedance spectroscopy on oxide films formed on zircaloy 4 in high temperature water, Electrochim. Acta 39 (1994) 455–465.
[40] F. Bentiss, H. Lagrenee, M. Traisnel, J.C. Hornez, The corrosion inhibition of mild steel in acidic media by a new triazole derivative, Corros. Sci. 41 (1999) 789–803.
[41] W.J. Lorenz, F. Mansfeld, Determination of corrosion rates by electrochemical DC and AC methods, Corros. Sci. 21 (1981) 647–672.
[42] G.T. Burstein, C. Liu, The cathodic reaction during repassivation of aluminium in open circuit, Corros. Sci. 37 (1995) 1151–1162.
[43] R. Kelly et al., Electrochemical Techniques in Corrosion Science and Engineering, Dekker, 2002. p. 45.
[44] D.A. Jones, Principles and Prevention of Corrosion, Macmillan, New York, 1992.
[45] P.J.F. Griffiths, J.D.R. Thomas, Calculations in Advanced Physical Chemistry, second ed., Edward Arnold, London, 1971.
[46] R.T. Foley, T.H. Nguyen, Chemical nature of aluminum corrosion, J. Electrochem. Soc. 129 (1982) 464–467.
[47] A.M. Al-Mayouf, Amino acids as corrosion inhibitors for aluminium in acid-chloride solutions, Corros. Prev. Contr. 6 (1996) 68–74.
[48] F.P. Ford, G.T. Burstein, T.P. Hoar, Bare surface reaction rates and their relation to environment controlled cracking of aluminum alloys, J. Electrochem. Soc. 127 (1980) 1325–1331.
[49] E.E. Oguzie, B.N. Okolue, E.E. Ebenso, G.N. Onuoha, A.I. Onuchukwu, Evaluation of the inhibitory effect of methylene blue dye on the corrosion of aluminium in hydrochloric acid, Mater. Chem. Phys. 87 (2004) 394–401.
[50] E.E. Foad El-Sherbini, S.M. Abdel Wahaab, M. Deyab, Ethoxylated fatty acids as inhibitors for the corrosion of zinc in acid media, Mater. Chem. Phys. 89 (2005) 183–191.
[51] M.S. Morad, A.M. Kamal El-Dean, 2,2′-Dithiobis(3-cyano-4,6-dimethylpyridine): a new class of acid corrosion inhibitors for mild steel, Corros. Sci. 48 (2006) 3398–3412.

[52] S. Gharebaa, S. Omanovic, Interaction of 12-aminododecanoic acid with a carbon steel surface. Towards the development of green corrosion inhibitors, Corros. Sci. 52 (2010) 2104–2113.
[53] T. Sethi, A. Chaturvedi, R.K. Updhyay, S.P. Mathur, Corrosion inhibitory effects of some schiffs bases on mild steel in acidic media, J. Chil. Chem. Soc. 52 (2007) 1206–1213.
[54] M.A. Migahed, H.M. Mohammed, A.M. Al-Sabagh, Corrosion inhibition of H-11 type carbon steel in 1 M hydrochloric acid solution by N-propyl amino lauryl amide and its ethoxylated derivatives, Mater. Chem. Phys. 80 (2003) 169–175.
[55] S. Bilgic, M. Sahin, The corrosion inhibition of austenitic chromium–nickel steel in H_2SO_4 by 2-butyn-1-ol, Mater. Chem. Phys. 70 (2001) 290–295.
[56] G. Gece, The use of quantum chemical methods in corrosion inhibitor studies, Corros. Sci. 50 (2008) 2981–2992.
[57] K. Fukui, Theory of Orientation and Stereoselection, Springer-Verlag, New York, 1975.
[58] V.S. Sastri, J.R. Perumareddi, Molecular orbital theoretical studies of some organic corrosion inhibitors, Corrosion 53 (1997) 617–621.
[59] I. Lukovits, E. Kálmán, F. Zucchi, LKP model of the inhibition mechanism of thiourea compounds, Corrosion 57 (2001) 3–7.
[60] N. Khalil, Quantum chemical approach of corrosion inhibition, Electrochim. Acta 48 (2003) 2635–2640.
[61] F. Bentis, M. Traisnel, H. Vezin, H.F. Hildebrand, M. Lagrenée, 2,5-Bis(4-dimethylaminophenyl)-1,3,4-oxadiazole and 2,5-bis(4-dimethylaminophenyl)-1,3,4-thiadiazole as corrosion inhibitors for mild steel in acidic media, Corros. Sci. 46 (2004) 2781–2792.
[62] V.S. Agarwal, K.C. Tripathi, Z. Phys. Chem. Leipzig 234 (1967) 397.
[63] S. Martínez, I. Štagljar, Correlation between the molecular structure and the corrosion inhibition efficiency of chestnut tannin in acidic solutions, J. Mol. Struct. (THEOCHEM) 640 (2003) 167–174.
[64] R.L. Pecsok, L.D. Shields, Modern Methods of Chemical Analysis, Wiley, NY, 1968. p. 241.
[65] R. Parr, W. Yang, Density functional approach to the frontier-electron theory of chemical reactivity, J. Am. Chem. Soc. 106 (1984) 4049–4050.
[66] R.S. Mulliken, Electronic population analysis on LCAO-MO molecular wave functions, J. Chem. Phys. 23 (1955) 1833–1840.
[67] F.L. Hirshfeld, Bonded-atom fragments for describing molecular charge densities, Theor. Chim. Acta B44 (1977) 129–138.
[68] C. Lee, W. Yang, R.G. Parr, Local softness and chemical reactivity in the molecules CO, SCN^- and H_2CO, J. Mol. Struct. (THEOCHEM) 163 (1988) 305–313.
[69] H. Sun, COMPASS: an ab initio force-field optimized for condensed-phase applications – overview with details on alkane and benzene compounds, J. Phys. Chem. B 102 (1998) 7338–7364.
[70] H. Andersen, Molecular dynamics simulations at constant pressure and/or temperature, J. Chem. Phys. 72 (1980) 2384–2393.
[71] M.P. Allen, D.J. Tildesley, Computer Simulation of Liquids, Clarendon Press, Oxford, 1987.
[72] J. Liu, W. Yu, J. Zhang, S. Hu, L. You, G. Qiao, Molecular modeling study on inhibition performance of imidazolines for mild steel in CO_2 corrosion, Appl. Surf. Sci. 256 (2010) 4729–4733.
[73] S. Xia, M. Qiu, L. Yu, F. Liu, H. Zhao, Molecular dynamics and density functional theory study on relationship between structure of imidazoline derivatives and inhibition performance, Corros. Sci. 50 (2008) 2021–2029.
[74] G.E. Brown, Chem. Rev. 99 (1999) 647.
[75] H. Hohl, M. Stumm, Interaction of Pb^{2+} with hydrous γ-Al_2O_3, J. Colloid Int. Sci. 55 (1976) 281–288.
[76] R. Wood, D. Formasiero, J. Ralston, Electrochemistry of the boehmite–water interface, Colloid Surf. 51 (1990) 389–403.
[77] K.C. Emregul, O. Atakol, Corrosion inhibition of iron in 1 M HCl solution with Schiff base compounds and derivatives, Mater. Chem. Phys. 83 (2004) 373–379.